Jurnal Kolaborasi
Sains dan Ilmu Terapan
Volume 5 No 1.1 Spesial Issue Agustus 2026 | Page 72-81
ISSN 2964- 5581 (media online)
https://utilityprojectsolution.org/ejournal/index.php/JuKSIT Penerbit : Cv. Utility Project Solutio

Performance Based Structural Analysis of a Bulk Carrier Pier Using Soil Structure Interaction Modeling

Irwansyah[1], Muhammad Sigit Darmawan[2*], Nur Achmad Husin[3], Kohar Yudoprasetyo[4]

[1,2,3,4)]Civil Infrastructure Engineering, Institut Teknologi Sepuluh Nopember, Surabaya, Indonesia

Email: [1]3035221002@student.its.ac.id, [2]m_sigit_d@its.ac.id, [3]na_husin@its.ac.id, [4]kohar.yudo@its.ac.id
Corresponding author: [2]m_sigit_d@its.ac.id

Info Artikel

Keywords:
Bulk Carrier Wharf
Soil-Structure Interaction
Virtual Fixity
Steel Pipe Pile
Pushover Analysis
Performance-Based Design

Abstract

Accurate representation of pile-soil interaction is essential for performance-based assessment c pile-supported wharves because lateral resistance, effective fixity, and plastic-hinge developmer depend strongly on surrounding soil conditions. This study compares a conventional virtua fixity-point (VFP) idealization with a calibrated soil-structure interaction (SSI) model for a bul carrier wharf in Gresik, Indonesia. Three models were evaluated: the existing wharf with VF supports, the same structure with distributed SSI springs, and an optimized SSI model wit reduced steel-pipe-pile diameters. The 20 m-wide platform was modeled in SAP2000 unde operational, berthing, mooring, environmental, and seismic loads. Lateral springs were derive from LPILE p-y analyses, assigned at 1 m depth intervals, and validated using pile-deflectio profiles under a 100 kN lateral load. Linear analysis evaluated demand-capacity ratios an serviceability displacements, while nonlinear pushover analysis used fiber hinges and strair based criteria. Relative to the VFP model, the SSI model reduced earthquake DCR from 0.648 t 0.548 and seismic displacement from 76.92 to 43.17 mm, while increasing performance-poir base shear by 27%. The optimized model reached a DCR of 0.770, and maximum pile strair remained within 19.2–21.0% of the Minimal Damage limit, confirming safer and more efficier structural optimization for comparable pile-supported marine infrastructure in seismic regions.

1. INTRODUCTION

Pile-supported wharves are critical links in maritime logistics because they must remain functional while resisting combinations of gravity, crane, berthing, mooring, current, wave, wind, and seismic actions. Their response is dominated by lateral deformation of long piles extending through the water column and into layered seabed deposits. Consequently, the assumed boundary condition below the seabed can strongly affect member forces, deck displacement, plastic-hinge locations, and the apparent reserve capacity of the complete wharf system.

Conventional design frequently replaces the embedded pile-soil continuum with an equivalent point of fixity. This virtual-fixity-point (VFP) approach is efficient and remains useful for preliminary analysis; however, it condenses depth-dependent soil resistance into a single boundary condition. Recent research has increasingly emphasized distributed pile-soil models. An earlier Indonesian assessment showed that soil slope and waveform duration influence the seismic response of wide pile-supported wharves [1], [2]. Three-dimensional simulations have also shown that soil deformation mechanisms and near-fault pulse characteristics influence displacement, axial force, and pile bending demand [3], [4], while nonlinear soil-pile-structure interaction can alter failure modes and the sequence of plastic-hinge formation in marine jetties [5], [6]. Quasi-static cyclic tests further indicate that loading direction, embedment, and pile position govern bending-moment and strain-energy concentration within pile groups [4]. Studies of isolated and conventional wharves similarly demonstrate that pile-soil interaction must be represented when evaluating seismic demand at different hazard levels [7], [8].

The direction and magnitude of SSI effects are not universal. They depend on soil stratigraphy, spring formulation, axial-lateral coupling, free pile length, pile diameter, and the reference simplification used for comparison. An Indonesian study in medium sand reported larger deformation and force demand from spring-based SSI than from a fixity-point

Submitted: **29/05/2026**; Accepted: **20/06/2026**; Published:**08/08/2026**

Jurnal Kolaborasi
Sains dan Ilmu Terapan
Volume 5 No 1.1 Spesial Issue Agustus 2026 | Page 72-81
ISSN 2964- 5581 (media online)
https://utilityprojectsolution.org/ejournal/index.php/JuKSIT Penerbit : Cv. Utility Project Solutio

model [9]. Conversely, calibrated stiff-clay resistance may increase effective lateral restraint and reduce deck deformation. Recent numerical work on pile groups in soft clay confirms that nonlinear soil constitutive assumptions are central to reproducing seismic behaviour [10]. In liquefiable deposits, excess pore pressure, interface contact, and pile-group position can substantially change settlement and bending-moment distributions [11]. Layered-soil analyses also identify earthquake intensity and the proportion of pile length embedded in weak strata as governing variables in kinematic interaction [12]. Variable pile-length modelling further shows that pile-group interaction changes stress overlap and settlement distribution [13]. The growing use of data-driven methods for offshore pile response reflects the limitations of overly simplified p-y representations [14].

Performance-based assessment provides a rational framework for resolving these modelling differences because it evaluates not only elastic demand but also displacement capacity, material strain, and failure mechanism. Current wharf practice uses nonlinear static or dynamic analysis to check performance at operating, contingency, and design-level earthquakes. Simplified displacement-capacity and equivalent single-degree-of-freedom procedures remain useful for verification and fragility analysis [15], [16], but distributed-plasticity models offer a more direct basis for tracing yielding and strain demand. Fragility research demonstrates that SSI may reduce deck-displacement vulnerability while increasing local force or curvature vulnerability, depending on the component and damage state [17]. Marine exposure adds a time-dependent dimension: corrosion can reduce pile strength and ductility, increase seismic fragility, and promote brittle failure, while climate-related changes in temperature and humidity may accelerate deterioration [18], [19], [20]. Recent Indonesian work has also shown that SSI, soil type, and deterioration can jointly change jetty stiffness, capacity, and ductility [21].

This study investigates a 60,000 DWT bulk carrier wharf in Gresik, East Java. The research gap addressed is the limited quantitative evidence on how a VFP idealization and a calibrated, depth-dependent SSI model affect both linear design checks and nonlinear performance for the same full-scale wharf geometry. The contribution is threefold: (1) a direct comparison of existing VFP and SSI models using identical structural and load data; (2) validation of the SSI spring representation against LPILE pile-deflection profiles; and (3) performance-based verification of an optimized pile configuration using fiber hinges and material strain limits. The study therefore connects geotechnical modelling choice with structural safety, performance level, and section efficiency in a form directly applicable to engineering design practice.

2. RESEARCH METHOD

The case study is a platform-type bulk carrier wharf located in Gresik, East Java. The reinforced-concrete deck is 20 m wide and is supported by five transverse rows of vertical steel pipe piles at 5 m spacing. The deck elevation is +5.28 m, the existing seabed is approximately -11.0 m relative to low water, and dredging reaches -14.0 m on the seaward side. The existing pile system comprises an upper D1016 mm segment and a lower D1219 mm segment, both with a nominal wall thickness of 15.9 mm. The wharf supports a continuous ship unloader, mobile cranes, a 100t truck, and 100 t bollards.

Three principal models were prepared in SAP2000. Model I represents the existing structure with pile extensions below the seabed terminating at VFP depths calculated using the OCDI procedure [22]. Model II retains the existing geometry but replaces the VFP boundary with distributed horizontal and vertical springs. Model III uses the same SSI formulation while reducing D1219 piles to D1016 and D1016 piles to D813 to obtain a more efficient DCR. Figure 1 presents the SAP2000 global model and the two principal pile-foundation idealizations, while Table 1 summarizes their differences.

2.1. Design Ship, Environmental Data, and Loading

The design vessel has a nominal capacity of 60,000 DWT, a length overall of 238 m, breadth of 34 m, and full-load draft of 12.3 m. Site data adopted in the analyses included a maximum wind speed of 20 m/s, current velocity of 0.5 m/s, wave height of 0.5 m, and tidal range of approximately 3.0 m. Berthing energy was calculated as 472.81 kN m (48.25 t m). Mooring loads were obtained from wind and current actions on the full and empty vessel, with the empty-vessel transverse wind load governing at 93.65 t.

Submitted: 29/05/2026; Accepted: 20/06/2026; Published:08/08/2026

Jurnal Kolaborasi
Sains dan Ilmu Terapan
Volume 5 No 1.1 Spesial Issue Agustus 2026 | Page 72-81
ISSN 2964- 5581 (media online)
https://utilityprojectsolution.org/ejournal/index.php/JuKSIT Penerbit : Cv. Utility Project Solutio

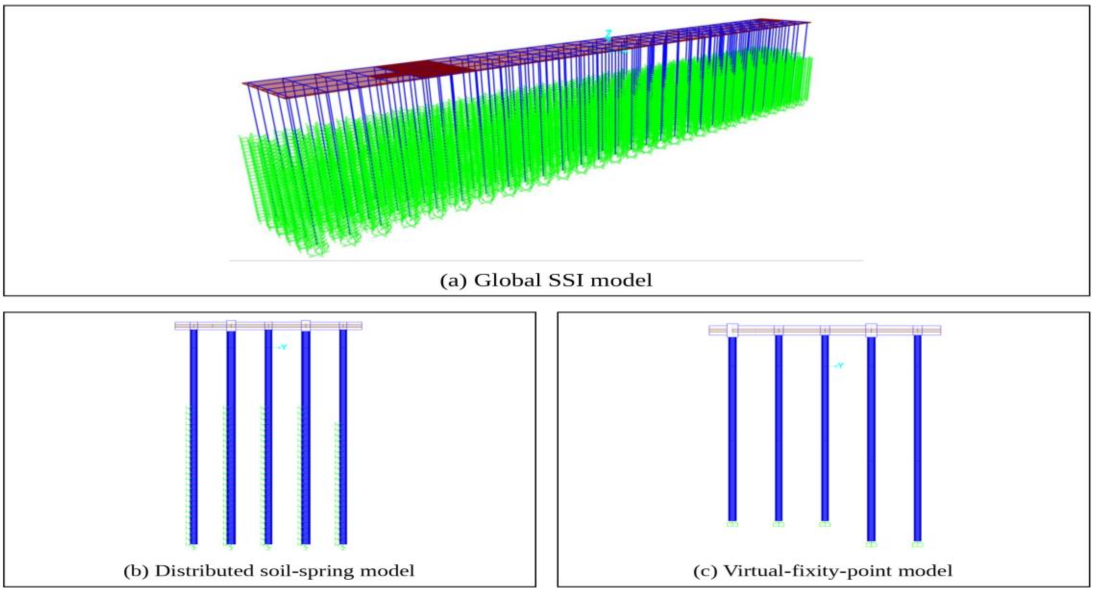

Figure 1. SAP2000 numerical idealizations: (a) global SSI model, (b) transverse frame with distributed soil springs, and (c) transverse frame using virtual fixity points

Table 1. Definition of the numerical models.

Model	Pile-soil representation	Crane-area pile	Non-crane pile	Purpose
I	Virtual fixity point	D1219	D1016	Existing-design reference
II	Distributed SSI springs	D1219	D1016	Effect of modelling method
III	Distributed SSI springs	D1016	D813	Section optimization

The principal operational loads were a 35 t/m continuous ship-unloader line load, an 11 t all-terrain-crane point load, a 16.4 t/m² crawler-crane area load, and the prescribed wheel/line/distributed components of a 100t truck. Earthquake demand used site class SD with PGA = 0.30 g, Ss = 0.60 g, S1 = 0.40 g, Fa = 1.20, Fv = 1.60, SDS = 0.48 g, and SD1 = 0.43 g. The seismic parameters and steel-member checks followed the Indonesian provisions adopted in the thesis [23], [24]. Linear serviceability checks followed the adopted BS 6349-2 limits [25]: 53.33 mm for operational horizontal displacement and 100 mm for earthquake displacement. The SAP2000 load-application schemes used for the SSI and VFP idealizations are presented in Figure 2.

Submitted: 29/05/2026; Accepted: 20/06/2026; Published:08/08/2026

Jurnal Kolaborasi
Sains dan Ilmu Terapan
Volume 5 No 1.1 Spesial Issue Agustus 2026 | Page 72-81
ISSN 2964- 5581 (media online)
https://utilityprojectsolution.org/ejournal/index.php/JuKSIT Penerbit : Cv. Utility Project Solutio

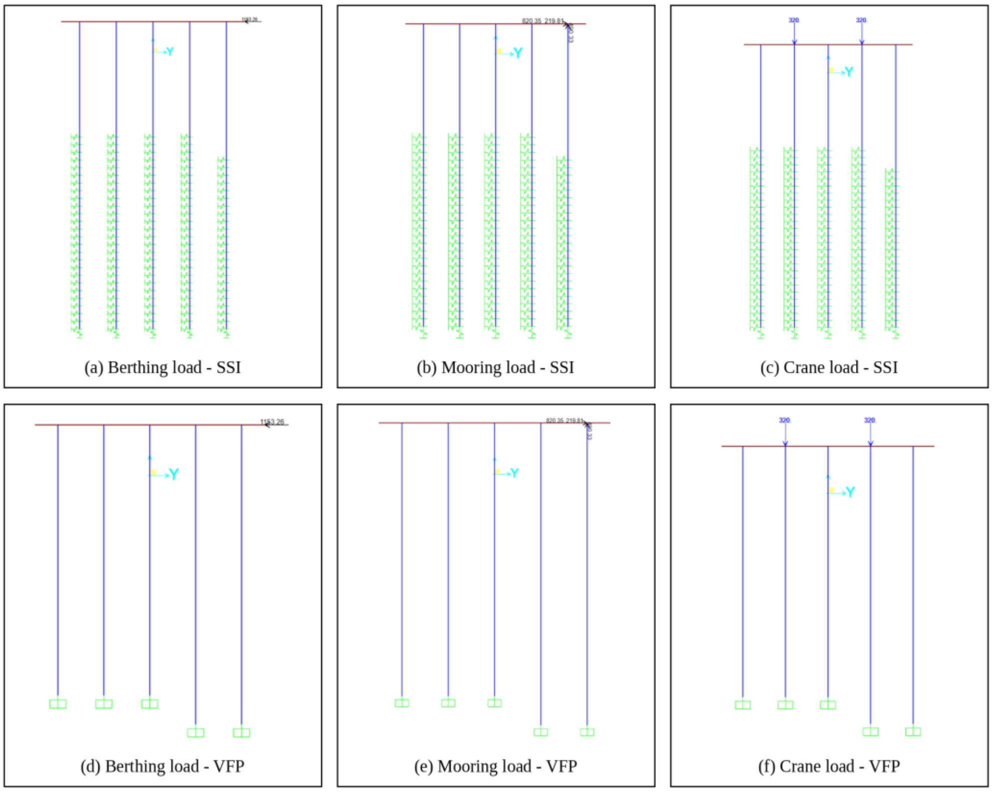

(a) Berthing load - SSI (b) Mooring load - SSI (c) Crane load - SSI
(d) Berthing load - VFP (e) Mooring load - VFP (f) Crane load - VFP

Figure 2. SAP2000 load application: (a-c) berthing, mooring, and crane actions in the SSI model; (d-f) corresponding actions in the VFP model

Table 2. Principal case-study parameters and applied actions.

Category	Parameter	Value
Geometry	Deck width; pile spacing	20 m; 5 m
Water levels	HWS; LWS; seabed	+3.0 m; 0.0 m; -11.0 m
Design vessel	DWT; LOA; breadth; draft	60,500 t; 238 m; 34 m; 12.3 m
Environment	Wind; current; wave; tide	20 m/s; 0.5 m/s; 0.5 m; 3.0 m
Berthing	Absorbed energy	472.81 kN m
Mooring	Governing transverse wind force	93.65 t (empty vessel)
Live load	CSU; crawler crane; truck	35 t/m; 16.4 t/m²; 100 t
Seismic	PGA; SDS; SD1	0.30 g; 0.48 g; 0.43 g

2.2. Soil Parameters and SSI Calibration

The geotechnical model was developed from boreholes BH03, BH04, and BH05 to 40 m depth. Representative N-SPT values of 29, 32, and 46 were correlated with undrained shear strengths of 145, 160, and 230 kPa and soil elastic moduli of 108.75, 120.00, and 172.50 MPa, respectively. Calculated elastic settlements were 18, 16, and 11 mm. These values were used to establish vertical spring response and to select the stiff-clay p-y formulation in LPILE.

Submitted: **29/05/2026**; Accepted: **20/06/2026**; Published:**08/08/2026**

Jurnal Kolaborasi
Sains dan Ilmu Terapan
Volume 5 No 1.1 Spesial Issue Agustus 2026 | Page 72-81
ISSN 2964- 5581 (media online)
https://utilityprojectsolution.org/ejournal/index.php/JuKSIT Penerbit : Cv. Utility Project Solutio

Horizontal soil resistance was calculated by pile diameter and depth. For each depth, a secant lateral stiffness was taken at 10 mm pile displacement, kh(z) = p(z)/0.010, and assigned as a discrete spring at 1 m intervals below the seabed. The calibrated stiffness increased with depth before approaching a plateau. For example, at 1 m below the seabed the D1016, D914, and D813 spring values were 33.87, 31.66, and 29.50 MN/m, while the corresponding plateau values were approximately 85.06, 78.31, and 71.64 MN/m. Vertical springs were iterated using kv = F/δ until the calculated elastic settlement was compatible with SAP2000 joint displacement.

The lateral SSI model was validated by applying an identical 100 kN horizontal load in SAP2000 and LPILE. The pile-deflection profiles differed by approximately 5%, which was accepted as convergence for the global structural analysis. This calibration step is important because p-y, t-z, and q-z representations can materially affect force distribution and plastic-hinge formation [5] [6]. Recent numerical studies further show that pile-soil interface contact, excess pore-pressure generation, layered-soil stiffness, and groundwater conditions can alter dynamic pile response [12], [11]. Figure 3 summarizes the adopted iterative procedure.

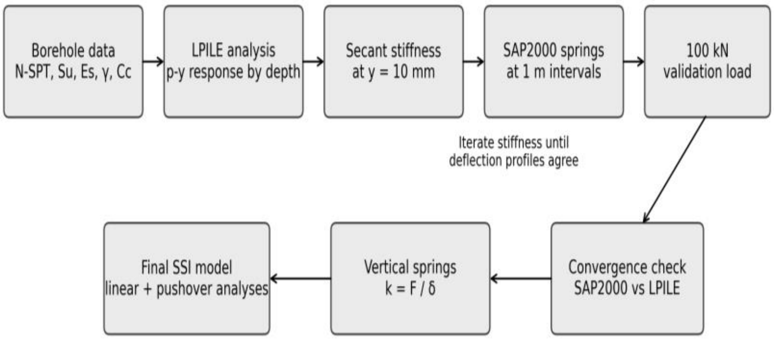

Figure 3. Calibration workflow for the soil-structure interaction model.

Table 3. Representative geotechnical and SSI parameters.

Parameter	BH03	BH04	BH05	Modelling use
N-SPT	29	32	46	Soil correlation
Undrained shear strength, Su (kPa)	145	160	230	Stiff-clay p-y model
Elastic modulus, Es (MPa)	108.75	120.00	172.50	Settlement and spring estimation
Compression index, Cc	0.30	0.30	0.30	Settlement calculation
Elastic settlement (mm)	18	16	11	Vertical-spring calibration
VFP depth range (m)	3.1-3.8	3.0-3.7	2.8-3.4	Model I boundary

2.3. Linear and Nonlinear Structural Analysis

Linear analyses were performed for ASD and LRFD combinations covering berthing, mooring, and earthquake conditions. Element adequacy was expressed by DCR = demand/capacity. The study adopted a working acceptance threshold of 0.95, while horizontal and vertical displacements were checked against the stated serviceability limits.

Nonlinear static pushover analyses were then conducted to determine the capacity curve, target displacement, strain demand, and hinge sequence. Steel pipe piles, including reinforced-concrete infill where present, were represented using fiber sections. Beam hinges were assigned using the SAP2000 auto-hinge formulation because the intended energy-dissipation mechanism was concentrated in the piles. Plastic-hinge lengths were approximately 0.83 m beneath the deck and 1.626, 1.828, 2.032, and 2.438 m at ground level for D813, D914, D1016, and D1219 piles, respectively. The use of fiber-section and nonlinear wharf models is consistent with prior three-dimensional simulations, multi-hazard performance evaluations, and cyclic model testing that explicitly tracked pile deformation and material demand [3]; [8].

Performance was evaluated using the material-strain limits adopted from ASCE/COPRI 61-14 and the Port of Long Beach Wharf Design Criteria [26] [27]. For the Minimal Damage/Operating Level Earthquake condition, the limiting strains were 0.010 for the steel pipe pile, 0.010 for concrete infill, and 0.015 for reinforcement. The intended wharf hierarchy permits controlled pile yielding while preserving the deck-beam system; accordingly, the beam-to-pile

Submitted: **29/05/2026**; Accepted: **20/06/2026**; Published:**08/08/2026**

capacity relationship was explicitly checked. The optimized Model III satisfied the adopted hierarchy at both critical locations, whereas the existing configurations did not.

3. RESULT AND DISCUSSION

3.1. Linear Demand-Capacity Ratio

All three models satisfied the adopted DCR limit for operational and earthquake conditions (Table 4 and Figure 4). Model I produced governing DCRs of 0.554 under operational loading and 0.648 under earthquake loading. Replacing the VFP boundary with calibrated SSI springs in Model II reduced these values to 0.429 and 0.548. Thus, for the same structural geometry, SSI reduced the maximum operational and earthquake DCRs by 22.6% and 15.4%, respectively.

The reduction indicates that the distributed stiff-clay springs provided greater effective lateral restraint than the equivalent VFP used in Model I. This result should not be generalized as an inherent consequence of SSI [9], for example, found that SSI increased demand relative to a fixity-point idealization for piles in medium sand. The contrast reinforces that SSI effects are conditional on soil profile, spring backbone, pile embedment, and the depth selected for equivalent fixity. A detailed model may be either more or less demanding than a simplified model; its value lies in representing the actual resistance distribution rather than applying a universal correction factor.

The optimized Model III increased the maximum operational and earthquake DCRs to 0.663 and 0.770. The earthquake DCR was 40.5% higher than that of Model II but remained 19% below the 0.95 study limit. This increase is desirable from a section-efficiency perspective because the reduced pile diameters mobilized more of the available strength without violating the acceptance criterion.

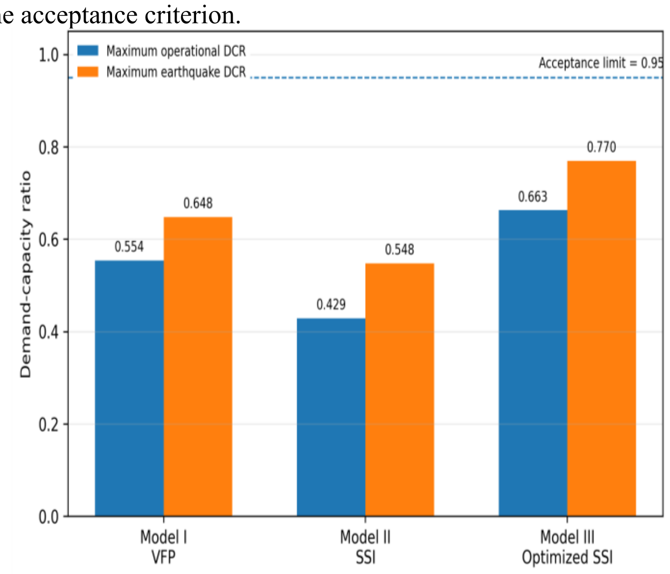

Figure 4. Governing DCRs from the linear analyses.

Table 4. Maximum linear response of Models I-III.

Model	Operational DCR	Earthquake DCR	Operational horizontal displacement (mm)	Earthquake horizontal displacement (mm)	Status
I - VFP	0.554	0.648	16.12	76.92	Safe
II - SSI	0.429	0.548	4.12	43.17	Safe
III - optimized SSI	0.663	0.770	16.82	46.35	Safe

3.2. Serviceability Displacement

Submitted: 29/05/2026; Accepted: 20/06/2026; Published:08/08/2026

Jurnal Kolaborasi
Sains dan Ilmu Terapan
Volume 5 No 1.1 Spesial Issue Agustus 2026 | Page 72-81
ISSN 2964- 5581 (media online)
https://utilityprojectsolution.org/ejournal/index.php/JuKSIT Penerbit : Cv. Utility Project Solutio

The modelling method had an even stronger effect on global displacement (Figure 5). Under berthing loading, the horizontal displacement decreased from 16.12 mm in Model I to 4.12 mm in Model II, a 74.4% reduction. Under earthquake loading, displacement decreased from 76.92 to 43.17 mm, a 43.9% reduction. The larger displacement sensitivity compared with the DCR sensitivity is expected because deformation integrates stiffness along the entire pile-soil system, whereas a member DCR is governed by the most critical local force-capacity combination.

Model III produced 16.82 mm under berthing and 46.35 mm under earthquake loading. Although the pile diameters were reduced, its seismic displacement was only 7.4% greater than Model II and remained less than half of the 100 mm limit. The result indicates that the soil springs continued to control the global deformation mode and that section reduction did not cause an unacceptable serviceability penalty. The supplementary Model IV, checked with the recalibrated R = Cd = 1.83, reached 70.21 mm and a maximum LRFD DCR of 0.80; both remained acceptable.

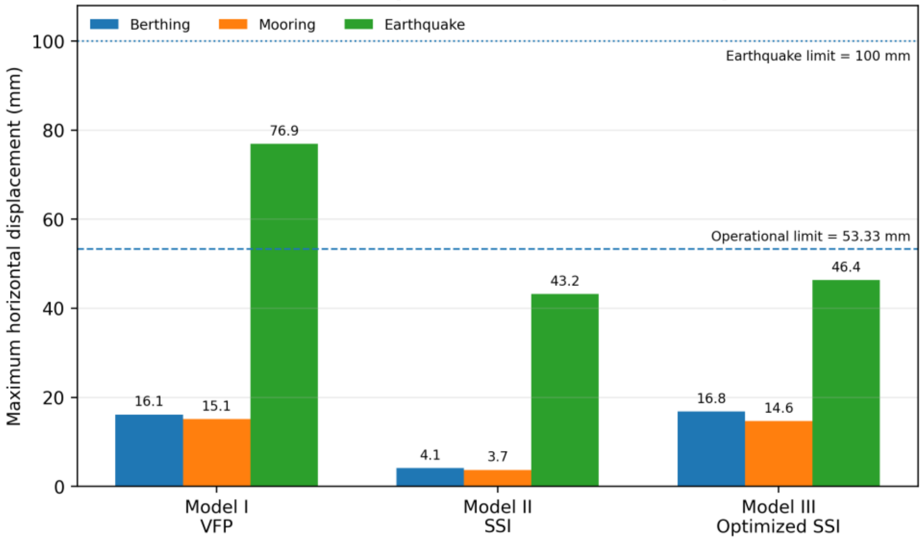

Figure 5. Maximum horizontal displacement under berthing, mooring, and earthquake actions

3.3. Pushover Capacity and Performance Point

The simplified capacity envelopes reconstructed from characteristic SAP2000 output points are shown in Figure 6. Model I remained approximately elastic to 0.52 m displacement and 115.97 MN base shear before reaching about 140 MN at 0.74 m. Model II showed a steeper initial response, reaching 173.80 MN at 0.48 m and an ultimate base shear near 198 MN at 0.60 m. The SSI model therefore increased the reported ultimate base shear by approximately 41.4% while reducing ultimate displacement, which is consistent with a stiffer global response.

At the capacity-spectrum performance point, Model I reached 34.13 MN at 0.151 m, whereas Model II reached 43.34 MN at 0.117 m. The calibrated SSI model therefore increased the performance-point base shear by 27.0% and reduced target displacement by 22.5%. This result confirms that the effect of SSI is not limited to elastic force redistribution; it also changes the location of the performance point and the deformation demand at which material strains must be evaluated.

The optimized Model III reached an elastic-stage point of approximately 121.04 MN at 0.58 m and an ultimate capacity near 127 MN at 0.62 m. Its lower capacity relative to Model II reflects the deliberate reduction of pile diameters. However, its reported performance point of 32.52 MN at 0.153 m remained well inside the strain-based acceptance limits. This balance between lower overstrength and acceptable deformation supports the optimization objective.

The observed increase in stiffness and base-shear capacity for the existing SSI model agrees with the broader conclusion that axial and lateral soil resistance can change the deformation and failure mode of marine jetties [5], [6]. It is also consistent with large-scale wharf studies showing that SSI significantly changes component fragility and that performance depends on hazard level, pile free length, and the selected response measure [17] [8]. The result complements the findings of[21], who showed that soil type controls both initial resistance and long-term ductility of marine jetty systems.

Jurnal Kolaborasi
Sains dan Ilmu Terapan
Volume 5 No 1.1 Spesial Issue Agustus 2026 | Page 72-81
ISSN 2964- 5581 (media online)
https://utilityprojectsolution.org/ejournal/index.php/JuKSIT
Penerbit : Cv. Utility Project Solutio

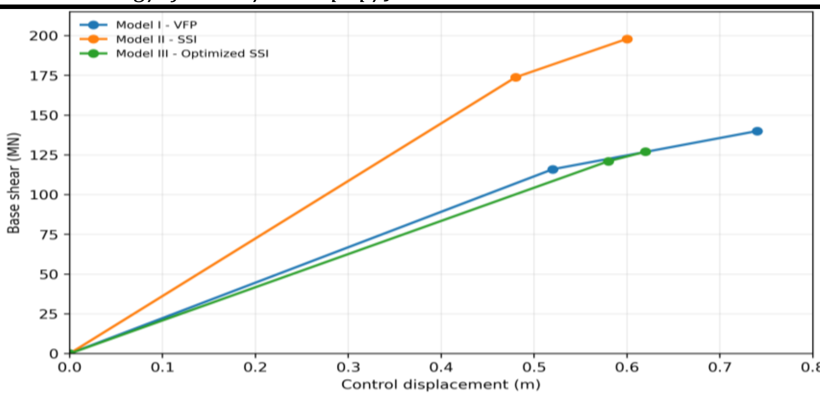

Figure 6. Simplified pushover envelopes reconstructed from the reported elastic and ultimate characteristic points

Table 5. Nonlinear performance indicators.

Model	Elastic-stage point, D/V	Ultimate point, D/V	Performance point, D/V	Max. pile-steel strain	Performance level
I - VFP	0.52 m / 115.97 MN	0.74 m / 140 MN	0.151 m / 34.13 MN	0.00197	Minimal Damage
II - SSI	0.48 m / 173.80 MN	0.60 m / 198 MN	0.117 m / 43.34 MN	0.00192	Minimal Damage
III - optimized SSI	0.58 m / 121.04 MN	0.62 m / 127 MN	0.153 m / 32.52 MN	0.00210	Minimal Damage

3.4. Material Strain and Plastic-Hinge Mechanism

The maximum steel-pile strains were 0.00197, 0.00192, and 0.00210 for Models I, II, and III. These correspond to utilization ratios of only 19.7%, 19.2%, and 21.0% against the 0.010 Minimal Damage limit (Figure 7). Concrete-infill strain utilization ranged from 3.0% to 6.6%, while reinforcement utilization ranged from 2.1% to 4.5%. All models were therefore classified as Minimal Damage under ASCE/COPRI 61-14, equivalent to the operating-level performance condition used by the Port of Long Beach criteria [26], [27].

The low strain utilization explains why all three models retained considerable reserve capacity even though their linear DCRs differed. It also demonstrates why DCR alone is insufficient for a performance-based conclusion: a model with a higher elastic demand can still exhibit acceptable nonlinear strain demand and a controlled mechanism. Conversely, a low DCR should not automatically be interpreted as optimal if it results from excessive pile dimensions.

Hinge progression also changed with the modelling method. In the detailed thesis output, first yielding occurred at step 8 for Model I and step 2 for Models II and III; the reported global collapse steps were 65, 9, and 32, respectively. The step numbers depend on load-step control and are not direct ductility indices, but they reveal that distributed soil restraint changed where and when yielding concentrated. Model III delayed global failure relative to Model II despite its smaller piles, consistent with the improved beam-to-pile capacity hierarchy.

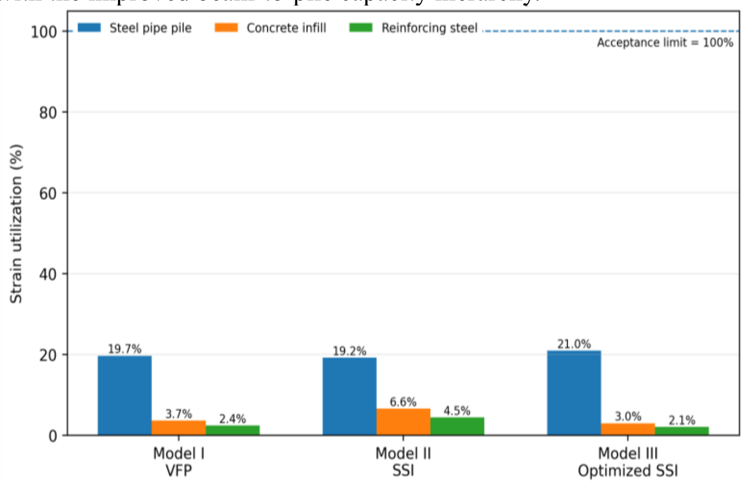

Figure 7. Material strain utilization at the evaluated performance state.

Submitted: **29/05/2026**; Accepted: **20/06/2026**; Published:**08/08/2026**

3.5. Engineering Implications and Limitations

For the investigated wharf, the VFP model was conservative in displacement and member demand relative to the calibrated stiff-clay SSI model. Using the VFP result alone could therefore encourage oversized piles and mask the potential for section optimization. The Model III results suggest that an earthquake DCR around 0.77-0.80 can be achieved while maintaining Minimal Damage performance. The practical implication is not that designers should target a single universal DCR, but that section efficiency should be assessed together with strain demand, displacement, and the intended plastic mechanism.

The results also show why independent calibration is essential. The 5% SAP2000-LPILE deflection agreement provides a defensible basis for the spring values, but the springs remain an idealization. The study did not include cyclic p-y degradation, gapping, liquefaction, scour, corrosion loss, group shadowing, or fully coupled kinematic interaction. Liquefaction studies demonstrate that pore-pressure accumulation and pile-soil contact can change both residual settlement and bending response [11], while corrosion studies show that section loss and random pitting progressively increase seismic vulnerability [18], [19], [20]. Pushover analysis also applies monotonic lateral loading and cannot reproduce record-to-record variability or cyclic accumulation. Recent near-fault, cyclic-test, and fragility studies demonstrate the importance of nonlinear time-history analysis for pulse effects, bidirectional demand, and repeated inelastic response [7], [4]. Consequently, the present findings are most appropriate for comparative design evaluation and should be extended with nonlinear dynamic analysis for final high-consequence seismic verification.

4. CONCLUSION

A calibrated distributed soil–structure interaction (SSI) model materially changed both the elastic and nonlinear responses of the Gresik bulk carrier wharf compared with the virtual-fixity-point idealization. For the identical existing geometry, the SSI model reduced the governing earthquake demand-capacity ratio from 0.648 to 0.548, corresponding to a reduction of approximately 15.4%, and decreased the horizontal seismic displacement from 76.92 mm to 43.17 mm, or approximately 43.9%. In the nonlinear analysis, the existing SSI model increased the performance-point base shear from 34.13 MN to 43.34 MN, representing an increase of approximately 27.0%, while reducing the target displacement from 0.151 m to 0.117 m, or approximately 22.5%. These results indicate that the SSI model produced a stiffer and stronger global structural response. The pile optimization applied in Model III increased the earthquake demand-capacity ratio to 0.770 and the seismic displacement to 46.35 mm; however, both values remained within the adopted performance limits, indicating that the optimized model utilized the available section capacity more efficiently than the existing SSI configuration. The maximum steel-pile strain ranged from 0.00192 to 0.00210, corresponding to only 19.2–21.0% of the Minimal Damage strain limit, and all evaluated models therefore satisfied the Minimal Damage or operating-level performance criterion. Nevertheless, the influence of SSI is dependent on the site conditions, soil profile, and modelling assumptions, meaning that the virtual-fixity-point approach may provide either conservative or unconservative predictions. Accordingly, equivalent-fixity designs should be verified using depth-dependent soil springs, while future studies should incorporate nonlinear time-history analysis and cyclic soil behaviour to provide a more comprehensive seismic performance assessment.

ACKNOWLEDGMENT

The authors acknowledge the Department of Civil Infrastructure Engineering, Institut Teknologi Sepuluh Nopember, for academic and technical support. The numerical data used in this manuscript were derived from Irwansyah's 2026 applied master's thesis. No external research funding was declared for this manuscript.

REFERENCES

[1] B. Christino and N. Takashi, "Seismic Performance Assessment of Wide Pile-Supported Wharf Considering Soil Slope and Waveform Duration," *SN Appl. Sci.*, 2021, doi: https://doi.org/10.3390/app12147266.

[2] B. Christino and N. Takashi, "Seismic Performance Assessment of Pile-Supported Wharfs:2D Frame Analysis Method Considering Both Inertial and Kinematic Forces," *SN Appl. Sci.*, 2021, doi: https://doi.org/10.3390/app13063629.

[3] S. Lei, L. Jinchl, E. Ahmed, and A. Arul, "Seismic performance of a pile-supported wharf: Three-dimensional finite element simulation," *Soil Dynamics and Earthquake Engineering*, 2017, doi: https://doi.org/10.1016/j.soildyn.2017.01.009.

[4] W. Jianfeng, S. Lei, X. Libo, and L. Xianzhang, "Seismic response analysis of pile-supported wharf under three types of near-fault ground motion," *structures*, 2024, doi: https://doi.org/10.1016/j.istruc.2023.105144.

Submitted: **29/05/2026**; Accepted: **20/06/2026**; Published:**08/08/2026**

[5] K. Marios, S. Panagiotis, M. Constantine, and O. Toula, "Numerical Study of the Nonlinear Soil Pile Structure Interaction Effects on the Lateral Response of Marine Jetties," 2024, doi: https://doi.org/10.3390/jmse12112075.
[6] K. Marios, M. Constantine, and O. Toula, "Nonlinear Soil Pile Structure Interaction Behaviour of Marine Jetty Structures," 2024, doi: https://doi.org/10.3390/jmse12071153.
[7] U. R. Sami, C. Yao, W. Zhuoxin, and Y. Ang, "Seismic performance assessment of pile supported wharves with seismic isolation system considering pile-soil interaction ," *ocean engineering*, 2024, doi: 10.1016/j.oceaneng.2024.119219.
[8] S. Lei, P. Hua, J. Wan, X. L. Lu, E. Ahmed, and K. A. Arul, "Seismic performance evaluation of a pile – supported wharf system at two seismic hazard level ," *ocean engineering*, 2021, doi: 10.1016/j.oceaneng.2020.108333.
[9] R. Kurniawan, A. S. Aprilia, M. Grace, C. A. Saputra, and A. A. Yufrizal, "Analysis of jetty structure using the fixity point method and soil-structure interaction via the spring model," *G-Tech: Jurnal Teknologi Terapan*, 2025, doi: https://doi.org/10.70609/g-tech.v9i3.6863.
[10] S. M. S. A. Jiankai *et al.*, "Seismic Behavior of Pile Group Foundations in Soft Clay:Insights from Nonlinear Numerical Modeling," *Infrastructures (Basel).*, 2025, doi: https://doi.org/10.3390/infrastructures10060134.
[11] Y. Yiliang, B. Xiaohua, L. Zhipeng, and C. Xiangsheng, "Dynamic Response of a Four Pile Group Foundation in Liquefiable Soil Considering Nonlinear Soil Pile Interaction," 2022, doi: https://doi.org/10.3390/jmse10081026.
[12] B. Selçuk and T. Haluk, "Numerical Investigation of the Pile Soil Interaction Problem under Dynamic Loads," 2023, doi: https://doi.org/10.3390/app132111653.
[13] H. Dongliang, C. Yanhui, L. Hongwei, and L. Hang, "Pile Soil Interaction and Group Pile Effect in Composite Foundation Under Different Pile Length Conditions," 2025, doi: https://doi.org/10.3390/buildings15081248.
[14] L. Peiyuan, L. Kun, Y. Xiangwei, L. Tong, Y. Xun, and L. Haoyi, "Analysis of Offshore Pile Soil Interaction Using Artificial Neural Network," 2025, doi: https://doi.org/10.3390/jmse13050986.
[15] Y. , Feng and S. Gao, "Seismic fragility analysis of concrete pile supported wharves based on single degree of freedom model. ," *SN Appl. Sci.*, 2022.
[16] G. Shufei, H. Zhenkun, and F. Yunfen, "Simplified Procedure for Estimating Seismic Displacement Capacity of Concrete Piles in Wharves," 2024, doi: https://doi.org/10.3390/buildings14123917.
[17] S. Lei, W. Hua-Ping, D. You, M. F. Dan, and L. Xian-Zhang, "Seismic fragility assessment of large-scale pile-supported wharf structures considering soil-pile interaction," 2019, doi: https://doi.org/10.1016/j.engstruct.2019.02.022.
[18] M. Hamid, A. Mohammad, Hariri-Ardebili, and M. Masoud, "Time-dependent seismic fragility analysis of corroded pile-supported wharves with updating limit states," *Soil Dynamics and Earthquake Engineering*, 2021, doi: https://doi.org/10.1016/j.soildyn.2020.106551.
[19] H. Mirzaeefard and M. A. Hariri-Ardebili, "The role of climate change and corrosion modeling strategy in dynamic response of pile supported wharves," *Soil Dynamics and Earthquake Engineering*, 2024, doi: https://doi.org/10.1016/j.soildyn.2024.108922.
[20] X. Zhao *et al.*, "Seismic fragility analysis of steel pipe pile wharves with random pitting corrosion," *Buildings*, 2023, doi: https://doi.org/10.3390/buildings13102619.
[21] M. S. Darmawan, K. Yudoprasetyo, A. N. Refani, M. F. Rosyidi, and Irwansyah, "Case study of the effect of soil structure interaction on marine jetty performance subjected to corrosion," 2026, doi: https://doi.org/10.21660/2026.141.5385.
[22] The Overseas Coastal Area Development Institute of Japan, "Technical Standard And Commentaries For Port And Harbour Facilities In Japan," 2002.
[23] Badan Standarisasi Nasional, *Tata Cara Perencanaan Ketahanan Gempa untuk Struktur Bangunan Gedung dan Nongedung*. 2019. [Online]. Available: www.bsn.go.id
[24] Badan Standarisasi Nasional, "SNI 1729 - 2020, Spesifikasi untuk Bangunan Gedung Baja Struktural," 2020.
[25] Bristish Standard, *Code of practice for the design of quay walls, jetties and dolphins*. 2019.
[26] American Society of Civil Engineers, *Seismic Design of Piers and Wharves*. United State of America, 2014.
[27] Port of Long Beach, *Wharf Design Criteria*. United State of America, 2021.

Submitted: **29/05/2026**; Accepted: **20/06/2026**; Published:**08/08/2026**